Simulation Study of Angular Resolution of a New Electromagnetic Sampling Calorimeter

Junlee Kim[1,], Eun-Joo Kim[1,], Young Jun Kim[1], Jung Keun Ahn[1], Gei Youb Lim[1]

[a]*Division of Science Education, Jeonbuk National University, Jeonju 54896, Korea*
[b]*Department of Physics, Korea University, Seoul 02841, Korea*
[c]*Institute of Particle and Nuclear Studies (IPNS), High Energy Accelerator Research Organization (KEK), Tsukuba 305-0801, Japan*

Abstract

We report simulation results on the angular resolution of electromagnetic (EM) sampling calorimeters with photons being in the range of 100 MeV to 2 GeV. A simulation model of the EM calorimeter consists of alternating layers of a 1-mm-thick Pb plate and a 5-mm-thick plastic scintillator plate. The scintillator plates are alternatively segmented in horizontal and vertical strips. In this study, we obtained energy deposit in individual strips using Geant4 simulations and reconstructed incident photon angles using a XGBoost model with boosted decision trees. Angular resolutions are studied in terms of the strip width. The 15-mm-wide strips provide the best angular resolution of $1.23 \pm 0.01^\circ$. Incident photon directions can be well reconstructed in the front part ($5X_0$) of the EM calorimeter. The angular resolution is almost constant for small angles less than 30°, and varies significantly with the incident photon energy. The energy dependence can be expressed as $\sigma_\theta = \text{xxx} \oplus \text{yyy} / \sqrt{E_\gamma}$.

Keywords: Electromagnetic Calorimeter, Geant4, XGBoost, KOTO

1. Motivation

The electromagnetic (EM) calorimeter plays an important role in experimental studies for the nuclear and particle physics. Various materials have been developed for better energy and timing resolutions so far [1]. EM calorimeters can be divided into two groups: sampling calorimeters and homogeneous calorimeter. Sampling calorimeters consist of alternating layers of an absorber generating EM showers and an active medium providing signals. On the other hand, homogeneous calorimeters are built of only a single type of material that facilitates both EM showers and signal

*Corresponding author. Tel.: +82-xxxxxxxxx.
**Corresponding author. Tel.: +82-xxxxxxxxx.

generations. Today, the sampling calorimeter becomes very popular in large-scale high energy experiments, owing to its cost-effectiveness. In sampling calorimeters the energy deposited in the active medium fluctuates because the active layers are interleaved with absorber layers. This so-called sampling fluctuation dominates the energy resolution.

The sampling fluctuation can be improved by optimizing the thickness ratio of the absorber to the active medium. A 3-m-long cylindrical calorimeter made of alternating layers of Pb and plastic scintillating plates is an example of the sampling calorimeter [2].

The segmented structure of the active medium facilitates the measurement of lateral distributions of the EM shower along the incident photon direction. The photon direction can also be deduced from the information on the EM shower shape. The measurement of photon directions can help predict photon production vertices, which is crucial for the background suppression in KOTO experiment [3].

Stochastic behaviors of the EM shower development limit to the angular resolution of the photon direction measurement. Energy deposits in each active layer of a sampling calorimeter fluctuate event by event so that the reconstruction of photon directions necessitates the longitudinal and lateral segmentation of the calorimeter.

This paper describes a machine learning approach based on XGBoost (XGB) model [4] with boosted decision trees in order to reconstruct the directions of incident photons entering a sampling calorimeter with alternating layers of a Pb plate and plastic scintillator strips in horizontal and vertical directions. We generated EM showers in a sampling calorimeter using Geant4 simulations. We report on the detector configuration providing the acceptable angular resolution, and report on the angular resolution of the EM sampling calorimeter in terms of the incident angle and energy.

2. Electromagnetic Shower Simulation

Simulation models of a sampling calorimeter were constructed as a block consisting of alternating layers of a 1-mm-thick Pb absorber and a 5-mm-thick polyvinyltoluene-based plastic scintillator. The plastic scintillator is segmented in 15-mm-wide strips, which is alternatively oriented in vertical and horizontal directions as shown in Fig. 1. The sampling calorimeter model has a cross-section of 525×525 mm^2 and accommodates 105 alternating layers of 630 mm length ($20X_0$), which is sufficiently long to absorb full photon energy in the range of 100 MeV to 2 GeV.

The detector response to incident photons was simulated using Geant4 (ver. 4.10.06) with the standard EM sub-packages [5]. The beam direction defines the z-axis. The photon direction is defined as polar angle (θ) with respect to the z-axis. Figure 2 illustrates simulated energy deposit patterns in each strip for a 1-GeV photon at a normal incidence in xz- and yz-planes. Each segmented region in Fig. 2

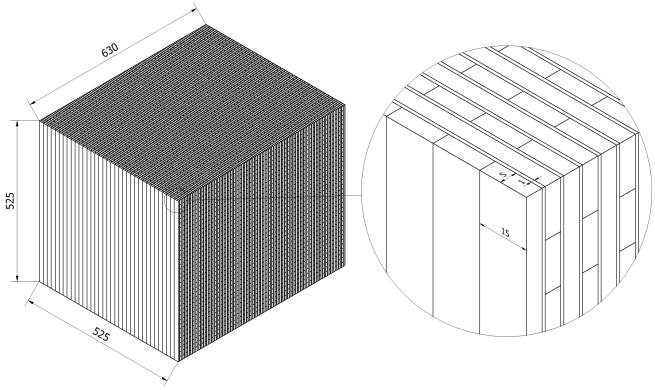

Figure 1: Schematic of the sampling calorimeter model consisting of 105 alternating layers of a Pb plate and a segmented scintillator plate in 35 strips. Each scintillator plate is oriented alternatively in horizontal and vertical directions. See text for details.

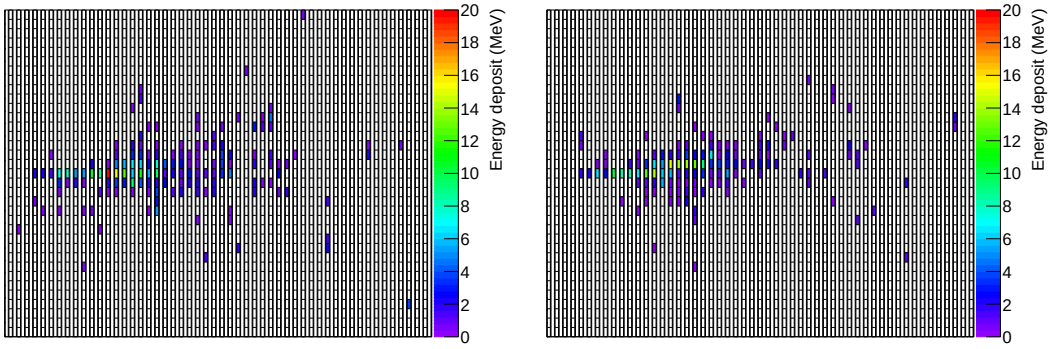

Figure 2: Event display of simulated energy deposit patterns for a 1-GeV photon entering the calorimeter ($\theta = 0$) in (a) xz- and (b) yz-planes.

represents each channel.

3. Reconstruction of Incidence Angles

Incidence angles of photons are reconstructed using the XGB model that is a scalable machine learning system for tree boosting [4]. A machine learning model maps a set of data inputs, known as features, to target variables. In this study, the XGB model maps a dataset of energy deposits in each scintillator strip to an incidence angle of a photon. Training data were carefully prepared using Geant4 simulation such that the input datasets are representative of a detector response of real sampling calorimeters. To minimize data bias, the incidence angles were uniformly generated at the detector surface in the angular range of $0 < \theta < 50^\circ$ and $0 < \varphi < 360^\circ$, where

φ denotes azimuthal angle. Such a wide angular coverage provides good training datasets for the XGB. The number of training samples is 10^5 considering limited computing resources. To test the reconstruction of incidence angles, we generated photons at a fixed incidence angle θ. Note that the incident energy is known.

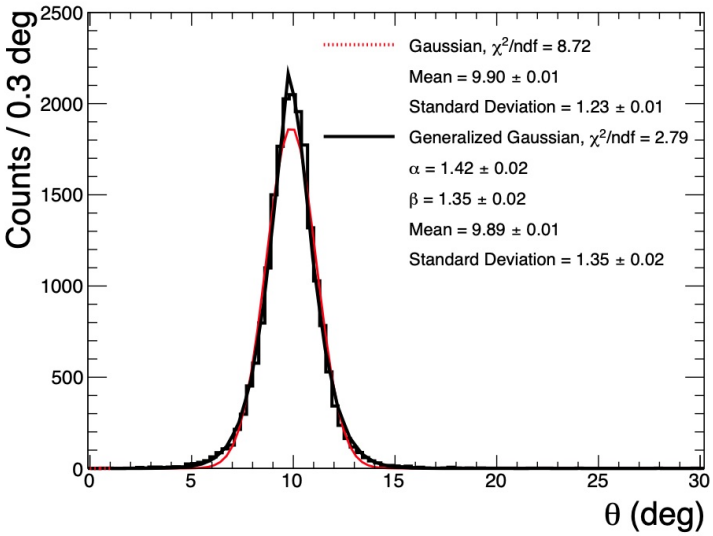

Figure 3: Reconstructed polar angle distribution for 1-GeV photons generated at $\theta = 10°$. The distribution is fitted with the Gaussian and the Generalized Gaussian function. The later gives a better result.

Figure 3 represents a distribution of reconstructed incidence angles θ for 1-GeV photons generated at $\theta = 10°$. The distribution is fitted with the Gaussian function and the Generalized Gaussian (GG) function. We tested two functions, Gaussian and GG to describe the reconstructed angle distribution. The GG function, also known as the generalized error distribution, is expressed as

$$f(x;\mu,\alpha,\beta) = \frac{\beta}{2\alpha\Gamma(1/\beta)} e^{-(|x-\mu|/\alpha)^\beta}, \tag{1}$$

where μ denotes a mean value. Parameters α and β determine the scale and shape of the distribution, respectively. Variance of the GG function is given by $\sigma^2 \equiv \alpha^2\Gamma(3/\beta)/\Gamma(1/\beta)$. The angular resolution of the incidence angle reconstruction is defined as σ.

We studied a correlation between byperparameters of the XGB model and the angular resolution. The test scans the evaluated angular resolution with different hyperparameters. Figure 4 shows the test results with N_estimators and Max. depth. N_estimators defines the maximum allowed number of decision trees to be developed, and the Max. depth defines the complexity of the structure of decision trees.

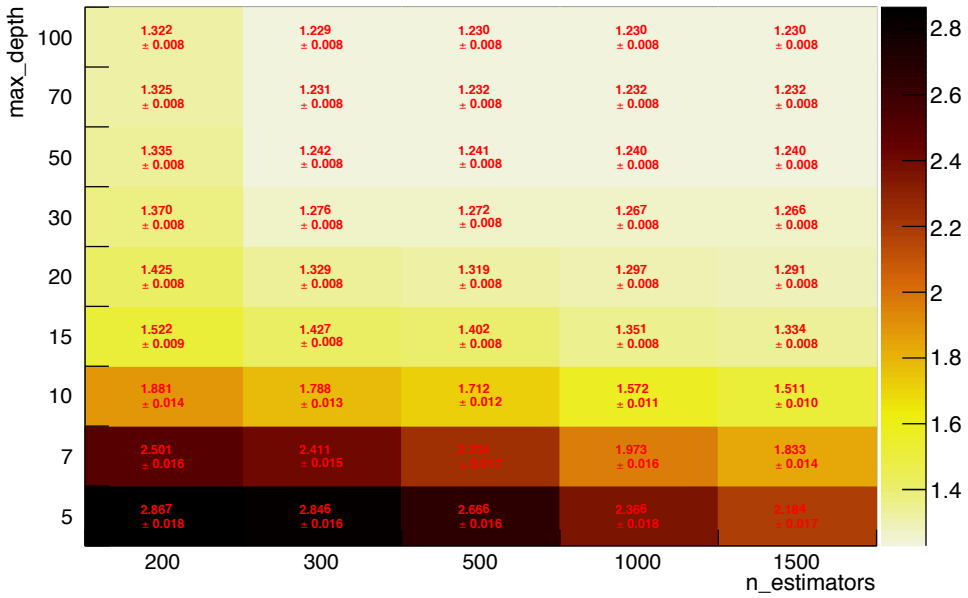

Figure 4: Angular resolutions are displayed in terms of combination of N_estimators and Max. depth. The best angular resolution is obtained with N_estimators = 300 and Max. depth = 100.

The best hyperparameter combination was searched for in terms of the angular resolution. As a results, N_estimators and Max. depth are set to 300 and 100, respectively. Similar tests were also performed for different hyperparameters. The best values for other hyperparameters are displayed in Tab 1. Other hyperparameters tuned in this study are Subsample, Learning rate, and Gamma. Subsample controls the fraction of total event samples for each boosting procedure, and Learning rate weights a decision tree to be added current model. Lastly, Gamma regulates the evaluation of each decision tree.

Table 1: Hyperparameters of the $XGBoost$

Parameter	Function	Default value	Used value
N_estimators	The number of decision trees	N.A.	300
Max. depth	Possible maximum depth of tree structure	6	100
Subsample	Fraction of total data used for a single decision	1	0.8
Learning rate	Step length for calculation	0.3	0.02
Gamma	Requirement on minimum loss function	0	0

Angular resolutions were deduced with varying strip widths from 5 mm to 35 mm as shown in Fig. 5. The 15-mm-wide strips yield the best angular resolution of

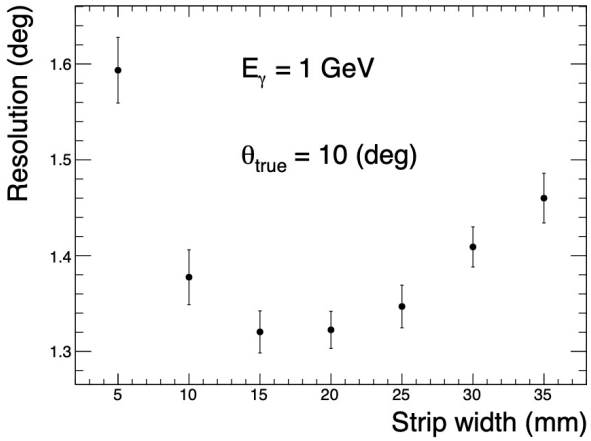

Figure 5: Angular resolutions are deduced in terms of the strip width for 1-GeV photons at $\theta = 10°$

1.23 ± 0.01°. The shorter the strip width is, the larger size of features, which can influence negatively in machine learning. For longer strips, the EM shower information can hardly be obtained.

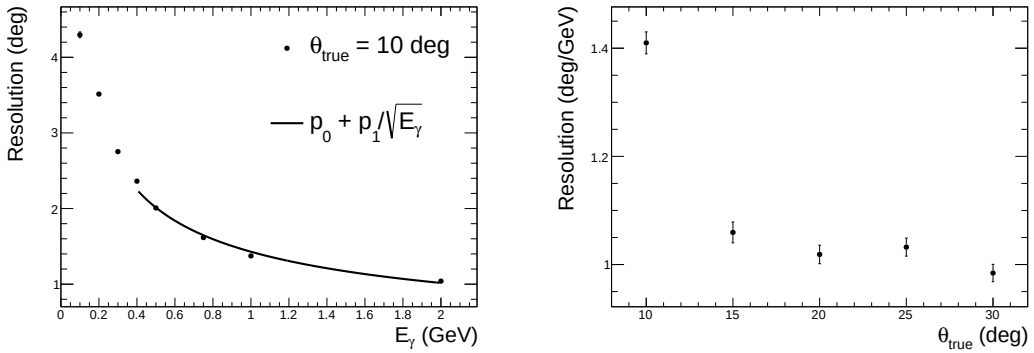

(a) (b)

Figure 6: Deduced angular resolutions as functions of (a) photon energy for $\theta = 10°$ and (b) polar angle for $E_\gamma = 1$ GeV.

Figure 6 (a) shows the angular resolution as a function of the incident photon energy (E_γ =) for $\theta = 10°$. Angular resolutions are fitted with a function of $p_0 \oplus p_1/\sqrt{E_\gamma(GeV)}$, where p_0 represents an energy-independent contribution and is estimated to be xxx, and p_1 denotes the energy-dependent parameter, mainly related with the development of the EM shower. p_1 is estimated to be xxx for $\theta > 15°$ and xxx° ± xxx° for $\theta = 10°$ in Fig. 6 (b). The discrepancy between them is attributed to the followings: polar angle to be always positive and poor angular resolutions for

low E_γ photons. When μ and α get comparable each other in Eq 1, the left tail of the distribution would extend to negative area. This largely affects the case $\mu = 10°$ and not the case $\mu > 15°$ considering that the angular resolutions for $E_\gamma = 0.1$ GeV is estimated to be 4°.

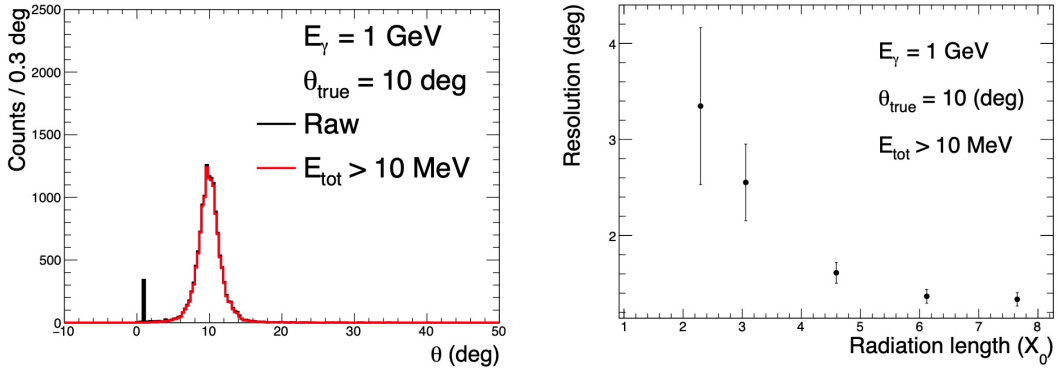

(a) (b)

Figure 7: (a) Reconstructed polar angles (θ) for 1-GeV photons at $\theta = 10°$. Red histogram represents the polar angle distribution by requiring $E_{\text{tot}} > 10$ MeV. (b) Angular resolution as a function of radiation length (X_0).

Furthermore, incidence angles are reconstructed with the front layers of X_0 in which 99% of incident photons generate EM showers. Figure 7 (a) shows reconstructed angles using front 24 layers of the detector, which corresponds to $4.6X_0$ for 1-GeV photons. A fraction of photons failed to be reconstructed due to the lack of active layers. The failed events are represented as a delta function near 0, and such events are removed by requiring the total energy deposit to be larger than 10 MeV. The angular resolution with the front layer is estimated to be XXX while possessing inefficiency estimated to be 5.8%.

Figure 8 shows the angular resolution with different numbers of training samples for different detector configurations. All configurations show a decrease in the angular resolution with increasing training samples, which means that enhanced statistics for the training results in better reconstruction. The angular resolution with 5-mm-wide scintillator strips decreases more rapidly than others. The number of features for the 5-mm-wide strip is much larger than others, and the number of training samples is much required to correlate larger features. Considering limited computing resources, the setup with 10^5 events, 24 layers, and the 15-mm-wide strip was chosen for training the $XGBoost$ model. The training result differs by only 0.1° from the best setup will full layers.

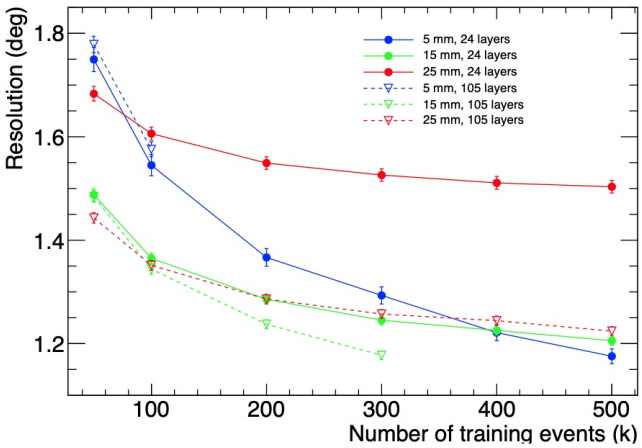

Figure 8: The angular resolution for 1-GeV photons at $\theta = 10^{\circ}$ as a function of the number of training samples with different strip widths using the first 24 layers or the full layers.

4. SUMMARY

We report simulation results on the incidece angle reconstruction of EM sampling calorimeters with photons being in the range of 100 MeV to 2 GeV. EM shwers are simulated in the new samplinng calorimeter.using Geant4. We utilize the $XGBoost$ model to reconstruct the photon incident angle by correlating all energy deposits in each strip with the incidence angle all events together.

We tune the hyperparameter of the $XGBoost$ to reconstruct the incidence angle with the best angular resolution, and study the angular resolution in terms of the detector configuration. We find that 15-mm-wide strips provide the best angular resolution, which can be expressed as $0.2 \oplus 1.1/\sqrt{E_\gamma}$ for different incident angles. We also conclude that using 24 front layers gives the angular resolution which is comparable with the angular resolution we get from the full layer.

We study that the angular resolution is changing with the variation of the training of the $XGBoost$ and the detector configuration. As the strip width decreases, more channels of scintillator strips are required, and the training of the $XGBoost$ gets affected due to the increased feature size. This is quenched with the larger number of training samples, which qualitatively improves the training of the $XGBoost$. On the other hand, the longer strip width provides the worse angular resolution as the position resolution of the EM shower gets worse. We conclude that 15-mm-wide strips provide the favorable angular resolution with 24 front layers and 10^5 training samples.

Acknowledgement

This paper was supported by the National Research Foundation of Korea (NRF) grants funded by the Korea government (MIST) (2019R1A2C1084552 and 2020R1A3B2079993).

References

[1] R.Wigmans, Prog. in Part. and Nucl. Phys. **103**, 109 (2018).

[2] R. Murayama et al., Nucl. Instrum. Meth. A **953**, 163255 (2020).

[3] T. Yamanaka and for the KOTO Collaboration (KOTO), PTEP **2012**, 02B006 (2012).

[4] T. Chen and C. Guestrin (2016), 1603.02754.

[5] S. Agostinelli et al., Nuclear Instruments and Methods in Physics Research Section A **506**, 250 (2003), ISSN 0168-9002.